Fibronectin adsorption on osteoconductive hydroxyapatite and non-osteoconductive α-alumina

Maki Hasegawa[1], Tada-aki Kudo[2], Hiroyasu Kanetaka[2], Toshiki Miyazaki[3], Masami Hashimoto[4] and Masakazu Kawashita[1]

[1] Graduate School of Biomedical Engineering, Tohoku University, Sendai 980-8579, Japan
[2] Graduate School of Dentistry, Tohoku University, Sendai 980-8575, Japan
[3] Graduate School of Life Science and Systems Engineering, Kyushu Institute of Technology, Kitakyushu 808-0196, Japan
[4] Japan Fine Ceramics Center, Nagoya 456-8587, Japan

E-mai1: m-kawa@ecei.tohoku.ac.jp

Keywords: adsorption, fibronectin, hydroxyapatite, α-alumina, osteoconductivity

Abstract. The osteoconductivity mechanism of hydroxyapatite (HAp) has not been elucidated. It is hypothesized that specific proteins absorb on HAp, promoting its osteoconductivity. To verify this hypothesis, we compared the adsorption behavior of fibronectin (Fn) on HAp powder and on α-alumina (α-Al_2O_3) powder, a material with no osteoconductivity. More Fn adsorbed on α-Al_2O_3 than on HAp, irrespective of the Fn concentration, and there was no significant difference in the secondary structure of Fn adsorbed on HAp and α-Al_2O_3. Further, it is possible that Fn did not adsorb on HAp and α-Al_2O_3 through the Arg-Gry-Asp motif of Fn. The amount of Fn adsorbed on HAp oriented to the a(b)-axis with very little carbonate decreased and the adsorbed Fn had a smaller α-helix structure content. The results suggest that the secondary and/or higher-order structure rather than the amount of adsorbed Fn might affect the osteoconductivity of HAp, which might be electrostatically controlled by crystal face orientation and/or carbonate content of HAp, although this should be confirmed by a cell culture test in the future.

1. Introduction

An ideal artificial bone material is readily available, has a low risk of infection, and is osteoconductive, i.e., it has the ability to serve as a scaffold for bone growth and bind to living bone directly [1]. Hydroxyapatite (HAp, $Ca_{10}(PO_4)_6(OH)_2$), the principal inorganic component in the mammal bone and tooth [2,3], is an osteoconductive material and artificial HAp is viable in the mammalian body over a long period [4–7]. In contrast, α-alumina (α-Al_2O_3) has high mechanical strength, abrasion resistance, corrosion resistance, and hydrophilicity, supporting its use as an artificial hip joint and artificial tooth root in humans since the 1970s [8]. However, α-Al_2O_3 is non-osteoconductive [9–11]. In addition, although the osteoconductivity of HAp has been verified, the fundamental mechanism is not fully understood. When an osteoconductive material is implanted on a living mammalian bone, osteoconduction occurs as follows: (1) protein adsorption from blood and tissue fluids, (2) mesenchymal cell recruitment, (3) attachment and proliferation of the mesenchymal cells, (4) osteoblast differentiation and osteoid production, (5) matrix calcification, and (6) bone remodeling [12,13]. Protein adsorbs on the artificial material in a living mammalian bone immediately, and the subsequent cell behavior depends on this process [12]. We previously hypothesized that a putative trigger protein first attaches to an implanted osteoconductive material, such as artificial HAp, and enhances bone formation and osseointegration in a living mammalian body. We then conducted studies to verify this hypothesis [14–16]. In these studies, a larger amount of bovine serum albumin (BSA)

adsorbed on α-Al_2O_3 compared to HAp [14,15]. In addition, BSA adsorbed on HAp induced different responses from mouse pre-osteoblastic MC3T3-E1 and mouse macrophage-like RAW264.7 cell lines compared to BSA adsorbed on α-Al_2O_3 [16]. BSA adsorption on α-Al_2O_3 was non-specific and involved electrostatic interaction, while that on HAp was specific and involved ionic interaction. Thus, there is a possibility that the specific adsorption of BSA on HAp might play a role in the induction of osteoconductivity.

Fibronectin (Fn) is a 440-kDa dimeric glycoprotein composed of two polypeptide chains [17], with a concentration of 140–380 $mg \cdot mL^{-1}$ (average of 330 $mg \cdot mL^{-1}$) in the living human body [18] and attaches to collagen and gelatin. Fn also binds to cells through integrins, which are representative transmembrane receptors for cell-cell and cell-extracellular matrix interactions [19]. Fn contains the Arg-Gly-Asp (RGD) motif, a tripeptide occurring in numerous proteins [20,21], in the cell-binding domains [18], and the RGD motif shows cell attachment activity [22] by electrostatic interaction with integrins [23]. In addition, the peptide-containing RGD motif (RGD-containing peptide) competitively inhibits direct interaction between Fn and the proteins that recognize the RGD motif of Fn [24–29], and the point-mutated non-polar peptide containing Arg-Gly-Glu (RGE) motif (RGE-containing peptide) is widely used as negative control peptide against the RGD-containing peptide [28,29]. These functional features of Fn affect the development of cartilage from mesenchymal cells in the mammalian bone formation process [18]. In mammals, most parts of the bone are formed by cartilage primordial formation, expansion, and cartilaginous ossification [30], suggesting that Fn plays an essential role in bone formation. Furthermore, Matsuno *et al.* implanted hydroxyapatite-immobilized collagen and fibronectin (HICF) and collagen-hydroxyapatite into full-thickness skull defects of rabbits and found that there were no significant differences in the numbers of cells attached to the disks, but cell pseudopodia developed at a noticeably faster rate on HICF disks than on collagen-hydroxyapatite [31]. Schönmeyr *et al.* investigated osteoblast attachment and proliferation on porous hydroxyapatite coated with fibronectin together with fetal calf serum [32]. In this study, *in vitro* attachment and proliferation of osteoblasts on porous hydroxyapatite was significantly increased by precoating with fibronectin together with fetal bovine serum [32]. Thus far, several studies have investigated the adsorption of Fn on HAp. For example, Dolatshahi-Pirouz *et al.* investigated the adsorption of Fn on an HAp-coated Au disc, using the uncoated Au disc as a reference [33]. The authors concluded that the detailed molecular structure of Fn and its functional activity depend significantly on both the underlying surface chemistry as well as the Fn surface coverage. Furthermore, Moraleda et al. investigated the influence of the surface features of HAp on the adsorption of Fn based on the hypothesis that the specific surface area (SSA), crystallite size (CS), and particle size (PS) affect the adsorption of proteins relevant to bone regeneration [34]. The study showed that Fn adsorption on HAp is not determined by a single parameter, and a combined analysis of the different parameters is necessary to design materials intended for protein interaction. It was also found that the combination of a large SSA and small CS favor the adsorption of Fn on HAp whereas the PS plays a modifying role.

However, the role of Fn as a putative trigger protein for osteoconduction is not well understood. In the present study, we compared the adsorption behavior of Fn on osteoconductive HAp and non-osteoconductive α-Al_2O_3 to gain further insight into a possible underlying mechanism through which Fn adsorption induces the osteoconductivity of HAp.

2. Materials and methods

2.1. Sample preparation

Commercially available HAp powder (ca-HAp; HAP-200, Taihei Chemical Industrial Co. Ltd., Japan), α-Al_2O_3 powder (ca-Al_2O_3; ALO14PB, Kojundo Chemical Lab. Co. Ltd., Japan), and Fn from bovine plasma (068-05703, Wako Pure Chemical Industries, Ltd., Japan) were used in the present study. In order to examine the effect of crystal orientation on Fn adsorption behavior, HAp powder orientated to the c-axis (a(b)-HAp) was prepared using the urea homogenous precipitation method [35,36] and those oriented to the a(b)-axis (c-HAp) were prepared according to Zhuang's method [36]. In addition, in order to investigate the adsorption site of Fn for ca-HAp or ca-Al_2O_3, carboxy fluorescein-aminohexyl amidite (FAM)-aminohexanoic acid (Ahx)-GRGDSP (K3038, Toray Research Center, Inc., Japan; purity: 95%, molecular weight: 1059.0) and FAM-Ahx-GRGESP (K3039, Toray Research Center, Inc.,

Japan; purity: 95%, molecular weight: 1073.1) peptides were used as RGD- and RGE-containing peptides, respectively. The FAM's excitation and emission wavelengths were 495 nm and 521 nm, respectively [37].

2.2. Sample characterization

The morphology of the samples was observed by scanning electron microscope (SEM; VE-8800, Keyence Corp., Japan). Crystalline phases of these materials were identified with an X-ray diffractometer (XRD; MiniFlex600, Rigaku Corp., Japan) with the following conditions: X-ray source, Cu-Kα, X-ray power, 40 kV, 15 mA, scanning rate, 2θ = 2 degree·min^{-1}, and sampling angle, 0.01 degree. The structure of HAp samples was investigated by Fourier-Transform Infrared spectroscopy (FT-IR; FT/IR-6200, Jasco Corp., Japan). For the FT-IR measurement, we used a potassium bromide (KBr) pellet method with a sample/KBr weight ratio of 1/800 at a resolution of 4 cm^{-1} and a cumulated number of 16. Samples HAps (ca-HAp, a(b)-HAp, and c-HAp) and ca-Al_2O_3 were previously heated for 2 h at 200 and 300°C, respectively, and the specific surface area (SSA) of these materials was measured using the Brunauer-Emmett-Teller (BET) technique (Autosurb®-iQ-MP, Quantachrome Instruments, USA). Commercially available bovine plasma Fn (068-05703, Wako Pure Chemical Industries, Ltd., Japan) was used in this study. The zeta potentials of the HAp samples, ca-Al_2O_3, and Fn in phosphate-buffered saline (PBS; 166-23555, Wako Pure Chemical Industries, Ltd., Japan) or PBS, including the synthetic RGD- or RGE-containing peptides at 35°C, were measured with electrophoresis spectroscopy (ELS-Z, Zetasizer Nano ZS90, Malvern Instruments Ltd., UK).

2.3. Measurement of Fn adsorption on samples

Fn was dissolved in PBS for 24 h at 4°C to obtain Fn solutions with different concentrations ranging from 0.10–0.45 mg·mL^{-1}. Tubes containing 5 mg ca-HAp and 11.5 mg ca-Al_2O_3 were incubated with 1.5 and 3.0 mL Fn solutions with different concentrations, respectively, at 36.5°C for 1 h while rotating at 5 rpm using a tube rotator (TR-350, As One Corp., Japan). The mixture was centrifuged for 10 min at 10,000 rpm (H-201F, Kokusan Co., Ltd., Japan), and the supernatant was collected by micropipette (Nichipet EXII, Nichiryo Co., Ltd., Japan). The supernatant (100 µL) was put into a 70 µL-disposable cell (UV-Cuvette micro, BrandTech Scientific Inc., UK) and the concentration of Fn in the supernatant was measured by a UV-Vis spectrometer (V-730BIO, Jasco Corp., Japan). For the Fn concentration measurement, the ultraviolet absorption method with optical path length of 10 mm was employed and the Fn concentration was estimated by the Warburg-Christian method [38]. The adsorbed amount of Fn was calculated using the Fn concentration in the supernatant. A similar measurement was performed for samples a(b)-HAp and c-HAp in 0.45 mg·mL^{-1} Fn solution.

The Hill equation was used for analysis of the Fn adsorption isotherm.

$$q = \frac{K_h C^n q_0}{1+K_h C^n} \quad (1)$$

where q is the amount of adsorption, q_0 is the saturated amount of adsorption, K_h is the equilibrium constant in the Hill model, C is the equilibrium concentration, and n is the Hill coefficient. The parameters K_h, q_0, and n were calculated using the ORIGIN software (Origin® 2015, Originlab Corp., U. S.) by nonlinear least-squares fitting to the adsorption isotherm data.

Further, the adsorption capacity of Fn on samples ca-HAp and ca-Al_2O_3 in Fn solutions with RGD-containing peptide or RGE-containing peptide (Fn-peptide mixed solutions) was measured. The concentrations of Fn and RGD- or RGE-containing peptide in the Fn-peptide mixed solutions were 0.15 mg·mL^{-1} and 0.1 µmol·mL^{-1}, respectively. The incubation conditions were the same as those described above but the incubation period was changed to 30 min. The concentration of RGD- or RGE-containing peptide ($C_{peptide}$) in the supernatant of the Fn-peptide mixed solutions after incubation was measured by fluorescence by exciting the peptide using visible-light at a wavelength of 495 nm. The concentration of proteins associated with Fn and peptides ($C_{protein}$) in the same supernatant were measured by a UV-Vis spectrometer in the manner described above. Then, the Fn concentration in the supernatant was estimated by subtracting $C_{peptide}$ from $C_{protein}$, and the adsorption capacity of Fn on the samples was calculated from the Fn concentration in the supernatant. The results are expressed as mean ± standard deviation. Statistical significance was set to $P < 0.05$ and was calculated using Student's t test.

2.4. Measurement of secondary structure of Fn adsorbed on the samples

The secondary structure of Fn adsorbed on the samples was measured by FT-IR spectroscopy as follows. Samples soaked in Fn solutions were freeze-dried (FD-1000, Tokyo Rikakikai, Tokyo). A moderate amount of the freeze-dried samples were placed on the KBr plate (2000-0060, Jasco, Tokyo) and pressed with another KBr plate at a pressure of 10 kN to form a KBr pellet 5 mm in diameter. The KBr pellet was subjected to FT-IR measurement at a resolution of 4 cm^{-1} and a cumulated number of 16. The absorption bands of Fn at 1600–1700 cm^{-1} were deconvoluted by principal components regression analysis using a protein secondary structure analysis software (IR SSE-4000, Jasco Corp., Japan).

3. Results and discussion

Figure 1 shows the XRD pattern of the samples a(b)-HAp, ca-HAp, c-HAp and ca-Al_2O_3. Samples ca-HAp, a(b)-HAp, and c-HAp had several XRD peaks ascribed to hydroxyapatite (PDF #01-071-5049). Samples a(b)-HAp and c-HAp showed high diffraction intensities of hydroxyapatite crystal faces (300) and (002), respectively, indicating that the expected crystal orientation of hydroxyapatite was achieved. Sample ca-Al_2O_3 had XRD peaks ascribed to α-Al_2O_3 (PDF #00-046-1212), indicating that the sample ca-Al_2O_3 contained no unwanted crystalline phases that may have affected the accuracy of the experimental results.

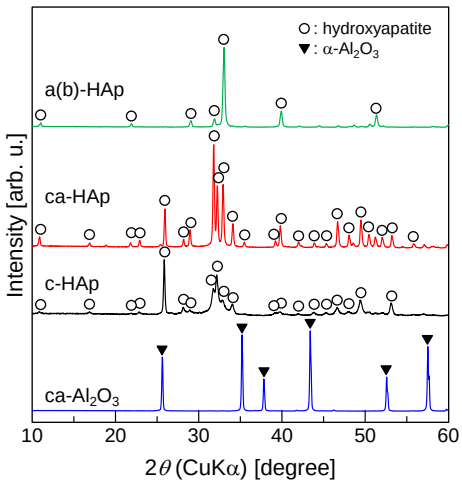

Figure 1. XRD patterns of samples a(b)-HAp, ca-HAp, c-HAp and ca-Al_2O_3.

Figure 2 shows the SEM images of the samples ca-HAp, ca-Al_2O_3, a(b)-HAp and c-HAp. Samples ca-HAp and ca-Al_2O_3 were composed of very fine particles that formed agglomerates and short chains. The agglomerates in samples ca-HAp and ca-Al_2O_3 had sizes ranging from 5–20 μm and 1–20 μm, respectively. Samples a(b)-HAp and c-HAp had rod- and a plate-like shapes, respectively. This remarkable difference in sample morphology can be attributed to the difference in hydroxyapatite crystal orientation in these samples, which was confirmed by the XRD analysis (Figure 1).

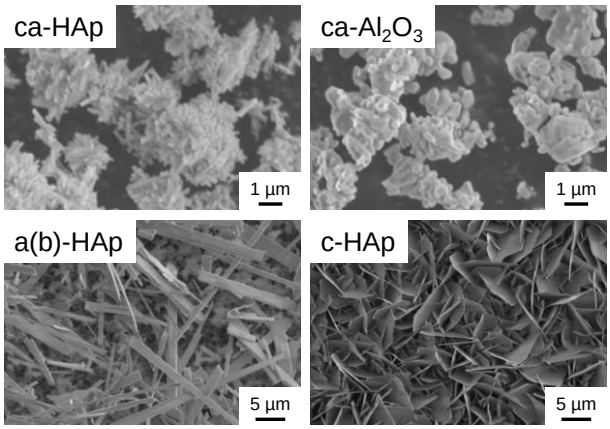

Figure 2. SEM images of samples ca-HAp, ca-Al_2O_3, a(b)-HAp and c-HAp.

Figure 3 shows the FT-IR spectra of samples a(b)-HAp, ca-HAp, and c-HAp. As shown in Figure 3(a), all samples had FT-IR absorption bands ascribed to phosphate (PO_4^{3-}), carbonate (CO_3^{2-}), the hydroxyl group (OH^-), and adsorbed H_2O [39–41]. The absorption bands of CO_3^{2-} were observed for samples a(b)-HAp and ca-HAp but not for sample c-HAp, indicating that samples a(b)-HAp and ca-HAp contained CO_3^{2-} but sample c-HAp contained very little CO_3^{2-} [40,41]. Figure 3(b) shows the FT-IR spectra of samples in wavenumbers ranging from 1300–1600 cm^{-1}. The absorption bands could be attributed to CO_3^{2-} replacing PO_4^{3-} of the hydroxyapatite crystal (type B replacement) [40,41]. Table 1 shows the SSAs and zeta potentials of the samples and Fn in PBS. It can be seen from the zeta potential that HAp samples (ca-HAp, a(b)-HAp, and c-HAp) and Fn were negatively charged while α-Al_2O_3 was positively charged. The mass of ca-HAp and ca-Al_2O_3 used in the following Fn adsorption test was determined using the SSAs of ca-HAp and ca-Al_2O_3 so that ca-HAp and ca-Al_2O_3 had the same surface area of 0.04 m^2.

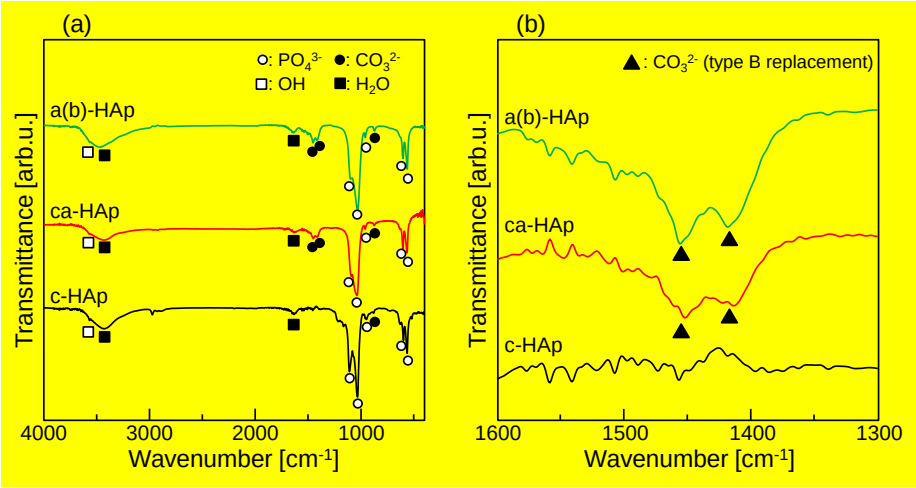

Figure 3. FT-IR spectra of samples a(b)-HAp, ca-HAp, and c-HAp, which were measured in different wavenumbers ((a): 400–4000 cm^{-1}, (b): 1300–1600 cm^{-1}).

Table 1. SSAs and zeta potentials of samples.

Sample	SSA [$m^2 \cdot g^{-1}$]	Zeta potential [mV]
ca-HAp	8.3	-13.8
ca-Al_2O_3	3.6	1.70
(a)b-HAp	5.1	-7.01
c-HAp	18.9	-29.1

Figure 4 shows the amount of Fn adsorbed on samples ca-HAp and ca-Al_2O_3 as a function of Fn

concentration ranging from 0.10–0.45 mg·mL^{-1}. Sample ca-HAp showed higher Fn adsorption capability (1.77–4.10 mg·m^{-2}) than sample ca-Al_2O_3 (2.44–11.7 mg·m^{-2}), irrespective of the Fn solution concentration. The amount of Fn adsorbed on sample ca-HAp was almost constant at Fn concentrations between 0.10–0.45 mg·mL^{-1} and there was no significant difference in the Fn adsorption capacity of ca-Al_2O_3 between the Fn concentrations of 0.35 mg·mL^{-1} and 0.45 mg·mL^{-1}. The Langmuir equation is often used for analysis of the adsorption isotherm, but when interactions between adsorbed proteins are not negligible, the Hill equation is used [33,42,43]. The determination coefficients (R^2) for the Fn adsorption isotherm on ca-HAp and ca-Al_2O_3 calculated using the Hill equation were 0.9857 and 0.9515, respectively, indicating that the Fn adsorption isotherm was well-approximated by the Hill equation. A Hill coefficient (n) larger than 1.0 (ca-HAp: 1.888, ca-Al_2O_3: 1.684) implies an attractive interaction between Fn adsorbed on both samples [33].

The higher adsorption capability of sample ca-Al_2O_3 compared to sample ca-HAp might be attributed to the electrostatic attraction between positively charged sample ca-Al_2O_3 and negatively charged Fn (Table 1). On the other hand, although electrostatic repulsion would have occurred between negatively charged sample ca-HAp and negatively charged Fn, certain amounts of Fn adsorbed on sample ca-HAp, implying that Fn can adsorb specifically on sample ca-HAp despite the electrostatic repulsion. Table 2 shows the secondary deconvoluted structure of Fn adsorbed on samples ca-HAp and ca-Al_2O_3. There was no significant difference in the secondary structure of Fn adsorbed on these samples. This result implies that the secondary structure of Fn has little influence on the Fn adsorption capacity of ca-HAp and ca-Al_2O_3.

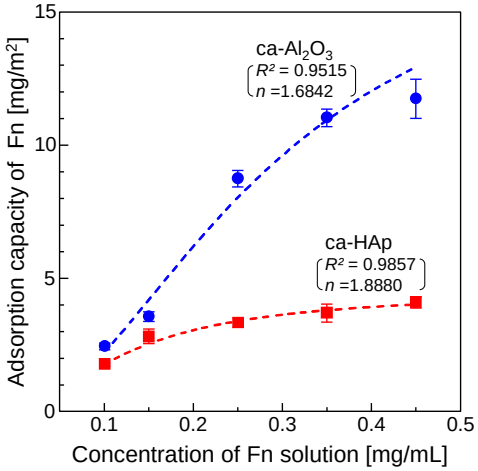

Figure 4. Adsorption capacity of Fn on samples ca-HAp and ca-Al_2O_3 as a function of Fn concentration of 0.10–0.45 mg·mL^{-1}.

Table 2. Secondary structure of Fn adsorbed on samples.

Sample	α-helix	β-sheet	β-turn	others
ca-HAp	15	34	24	27
ca-Al_2O_3	12	35	24	29
(a)b-HAp	13	35	25	27
c-HAp	3	43	22	32

Figure 5 shows the amount of Fn adsorbed on samples ca-HAp, a(b)-HAp, and c-HAp at an Fn concentration of 0.45 mg·mL^{-1}. There were significant differences in the Fn adsorption capacity of these samples and the order of Fn adsorption capacity was a(b)-HAp > HAp > c-HAp. Table 2 shows the secondary structure of Fn adsorbed on these samples. Interestingly, the content of the α-helix in Fn adsorbed on sample c-HAp was lower than those on samples ca-HAp and a(b)-HAp, which implies that Fn hardly denature on c-HAp. In fact, a previous study estimated 47% β-sheet, 28% turn, and 25% unordered structures, which were closer to those of Fn adsorbed on c-HAp than on other samples (Table 2), for non-adsorbed Fn in aqueous-buffered solution [44]. It has been reported that a small amount of α-helix structure [45] is contained in the collagen-binding domain [46], cell-binding

domain [47], and domain of unknown function [40] of Fn, and the calculated isoelectric points of these domains were 3.56–5.52 [45–48], indicating that these domains are negatively charged in the human body. In addition, Osterlund et al. reported that Fn denatured to change the β-sheet to an α-helix inversely [49]. Based on the present results and the above findings, we can speculate that Fn was denatured and the α-helix of Fn increased to adsorb on ca-HAp and a(b)-HAp. On the other hand, HAp has different atomic arrangements on the two types of crystal planes; a(b)-plane and c-plane. The difference between the a(b)-plane and the c-plane is as follows: the a(b)-plane is rich in calcium ions and is positively charged, while the c-plane is rich in phosphate and hydroxide ions and is negatively charged [50–52]. As shown in Figure 2, samples a(b)-HAp and c-HAp mainly had positively charged a(b)-planes and negatively charged c-planes, respectively. Therefore, the adhesion of negatively charged Fn was inhibited on c-HAp with a negatively charged c-face. Here, it is also noted that sample c-HAp is characterized by its extremely low content of carbonate (Figure 3). The difference in the carbonate content might change the charged state of the HAp crystal face [53], resulting in even lower adsorption capacity of Fn on c-HAp. The above results imply that the secondary and/or higher-order structure rather than the amount of adsorbed Fn plays an important role in the osteoconductivity of HAp and it is partially controlled by the crystal face orientation of HAp.

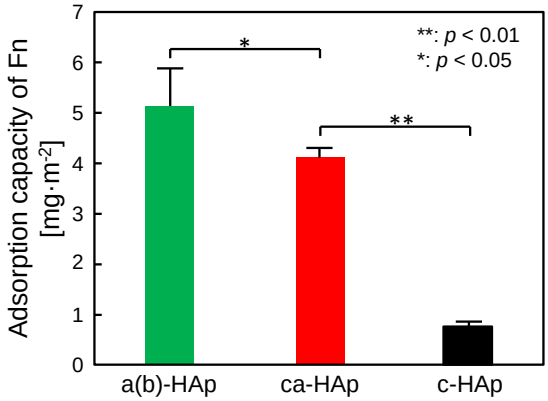

Figure 5. Adsorption capacity of Fn on samples ca-HAp, a(b)-HAp, and c-HAp at an Fn concentration of 0.45 mg·mL^{-1}.

Fn has an RGD motif in the cell attachment domain, which raises the possibility that Fn adsorbs on osteoconductive materials, such as HAp, to expose its RGD motif to osteoblasts and/or osteoclasts that mainly mediate bone formation and its remodeling. This is based on the assumption that HAp does not have the adsorption site of the RGD motif and/or Fn does not adsorb on the materials through the RGD motif. Therefore, adsorption behavior of Fn on samples ca-HAp and ca-Al_2O_3 in Fn solution with synthetic RGD-containing peptide (FAM-Ahx-GRGDSP, see Materials and methods for detail) and point-mutated RGE-containing peptide (FAM-Ahx-GRGESP, see Experimental for detail) without cell attachment activity (as reference) was investigated in the present study. If the Fn adsorbs on samples ca-HAp and ca-Al_2O_3 via the RGD motif, the adsorption behavior of Fn would remarkably change in Fn solution with RGD-containing peptide because the RGD motif in Fn becomes inactivated by the RGD-containing peptide. The Fn still showed negative zeta potentials in the solution with RGD- (–5.2 mV) or RGE-containing peptide (–7.4 mV), suggesting that the addition of RGD- or RGE-containing peptide hardly affects the surface charge of Fn in the solution. Figure 6 shows the adsorption capacity of Fn on these samples in Fn solution with RGD- or RGE-containing peptide. As described before, the RGD-containing peptide has been widely used as a competitive inhibitor of direct protein association with the RGD motif within Fn, and the RGE-containing peptide with non-polar characteristics has also been used as an inactive control peptide against RGD-containing peptide in previous studies. For each sample material (ca-HAp or ca-Al_2O_3) of the present study, the point-mutated and inactive RGE-containing peptides in Fn solution had no statistically significant effect on the adsorption capacity of Fn on the employed materials, compared to the parental and active RGD-containing peptides in Fn solution. The results suggest that Fn adsorbs on samples ca-HAp and ca-Al_2O_3 not via the RGD motif. Figure 7 shows a schema of possible adsorption of Fn on HAp based on the presumption that Fn adsorbs on HAp

though the collagen-binding domain but not the RGD motif of Fn. This schema was created based on the reported phenomenon that Fn binds to collagen *in vitro* [20,54]. As shown in this schema, the RDG motif might be exposed to enhance osteoblast and/or osteoclast cell adhesion, resulting in expression of osteoconductivity when Fn adsorbed on HAp. The above hypothesis will be confirmed by a cell culture test in the future.

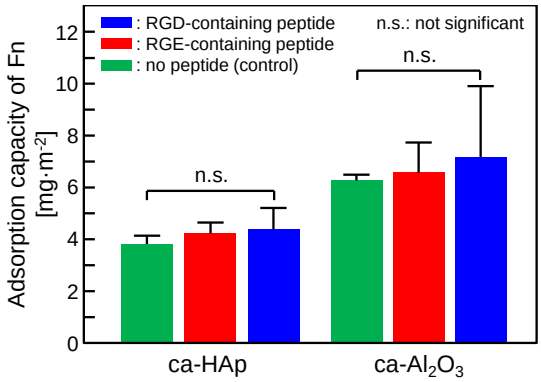

Figure 6. Adsorption capacity of Fn on samples ca-HAp and ca-Al_2O_3 in Fn solution with RGD-containing peptide, RGE-containing peptide, or no peptide.

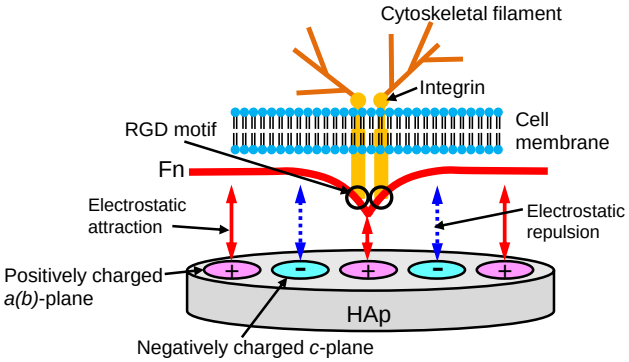

Figure 7. Schema of possible adsorption of Fn on HAp based on the presumption that Fn adsorbs on HAp though the collagen-binding domain.

4. Conclusions

We examined Fn adsorption on osteoconductive HAp and non-osteoconductive α-Al_2O_3. A larger amount of Fn adsorbed on α-Al_2O_3 than HAp irrespective of Fn concentration and there was no significant difference in secondary structure of Fn adsorbed on HAp and α-Al_2O_3. Further, we pharmacologically showed that Fn did not adsorb on HAp and α-Al_2O_3 through the RGD motif of Fn. On the other hand, the amount of Fn adsorbed on HAp oriented to the a(b)-axis (showing relatively lower carbonate content) decreased and the adsorbed Fn had a smaller α-helix structure content. Taken together, the present results suggest that the secondary and/or higher-order structure rather than the amount of adsorbed Fn might affect the osteoconductivity of HAp, which could be electrostatically controlled by crystal face orientation and/or the carbonate content of HAp, although this should be confirmed by a cell culture test in the future.

Acknowledgements

This work was partially supported by the Naito Foundation Natural Science Scholarship. The authors thank Dr. Tomoyuki Ogawa of Tohoku University for the zeta potential measurement, Dr. Masanobu Kamitakahara of Tohoku University for the specific surface area measurement, and Prof. Mamoru Aizawa of Meiji University for preparation of samples a(b)-HAp and c-HAp.

References

[1] LeGeros R Z 2002 *Clin. Orthop. Relat. Res.* **395** 81
[2] Dorozhkin S V and Epple M 2002 *Angew. Chem. Int. Ed.* **41** 3130
[3] Kuroda K and Okido M 2012 *Bioinorg. Chem. Appl.* 730693
[4] Singh S, Trikha S P, Edge A J 2004 *J. Bone Joint Surg. Br.* **86** 1118
[5] Trikha S P, Singh S, Raynham O W, Lewis J C, Mitchell P A and Edge A J *J. Bone Joint Surg. Br.* **87** 1055
[6] Adachi N, Ochi M, Deie M and Ito Y 2005 *J. Rheumatol.* **32** 1615
[7] Hurber F X, McArthur N, Hellmeier J, Kock H J, Baier M, Diwo M, Berger I and Meeder P J 2006 *Arch. Orthop. Trauma Surg.* **126** 533
[8] Ben-Nissan B, Choi A H and Cordingley R 2008 Alumina Ceramics *Bioceramics and Their Clinical Applications* ed T Kokubo (Cambridge: Woodhead Publishing) pp 223–242
[9] Stea S, Savarino L, Toni A, Sudanese A, Giunti A and Pizzoferato A 1992 *Biomaterials* **13** 664.
[10] Okada Y, Kobayashi M, Neo M, Shinzato S, Matsushita M, Kokubo T and Nakamura T 2000 *J. Biomed. Mater. Res.* **49** 106
[11] Tarique AA, Tsuru K, Maruta M, Takeuchi A, Matsuya S, Terada Y and Ishikawa K 2010 *J. Ceram. Soc. Japan* **118** 512
[12] Puleo D A and Nanci A, 1999 *Biomaterials* **20** 2311
[13] Nakamura M, Sekijima Y, Nakamura S, Kobayashi T, Niwa K and Yamashita K 2006 *J. Biomed. Mater. Res., Part A* **79A** 627
[14] Hayashi J, Kawashita M, Miyazaki T, Kamitakahara M, Ioku K and Kanetaka H 2012 *Phosphorus Res. Bull.* **26** 23
[15] Kawashita M, Hayashi J, Li Z, Miyazaki T, Hashimoto M, Hihara H and Kanetaka H 2014 *J. Mater. Sci.: Mater. Med.* **25** 453
[16] Kawashita M, Hayashi J, Kudo T, Kanetaka H, Li Z, Miyazaki T and Hashimoto M 2014 *J. Biomed. Mater. Res., Part A* **102A** 1880
[17] Engel J, Odermatt E, Engel A, Madri J A, Furthmayr H, Rohde H and Timpl R 1981 *J. Mol. Biol.* **150** 97
[18] Richard O H 1990 *Fibronectins* (New York: Springer) pp 24–25, pp 84–92
[19] Hynes R O 1987 *Cell* **48** 549
[20] Mao Y and Schwarzbauer J E 2005 *Matrix Biol.* **24** 389
[21] Ruoslahti E and Pierschbacher M D 1987 *Science* **238** 491
[22] Pierschbacher M D and Ruoslahti E, 1984 *Nature* **309** 30
[23] Ben-Ze'ev A, Farmer S R and Penman S, 1980 *Cell* **21** 365
[24] Aumailley M, Gurrath M, Müller G, Calvete J, Timpl R and Kessler H 1991 *FEBS letters* **291** 50
[25] Chen Q, Kinch M S, Lin T H, Burridge K and Juliano R L 1994 *J. Biol. Chem.* **269** 26602
[26] Koivunen E, Wang B and Ruoslahti E 1994 *J. Cell. Biol.* **124** 373
[27] Buckley C D, Pilling D, Henriquez N V, Parsonage G, Threlfall K, Scheel-Toellner D, Simmons D L, Akbar A N, Lord J M and Salmon M 1999 *Nature* **397** 534
[28] Erb L, Liu J, Ockerhausen J, Kong Q, Garrad R C, Griffin K, Neal C, Krugh B, Santiago-Pérez L I, González F A, Gresham H D, Turner J T and Weisman G A 2001 *J. Cell. Biol.* **153** 491
[29] Pebworth M P, Cismas S A and Asuri P 2014 *PLoS ONE* **9** e110453.
[30] Hall B K and Miyake T 2000 *BioEssays* **22** 138.
[31] Matsuno T, Uchimura E, Ohno T, Satoh T, Sugo Y, Ito A, Yamazaki A, Ishikawa Y, Kondo N and Ichinose N 2005 *Int. Cong. Series* **1284** 330
[32] Schönmeyr B H, Wong A K, Li S, Gewalli F, Cordiero P G and Mehrara B J 2008 *Plast. Reconstr. Surg.* **121** 751
[33] Dolatshahi-Pirouz A, Jensen T, Foss M, Chevallier J and Besenbacher F 2009 *Langmuir* **25** 2971
[34] Fernández-Montes Moraleda B, San Román J and Rodríguez-Lorenzo L M 2013 *J. Biomed. Mater. Res., Part A* **101A** 2332
[35] Wang Y, Yan Y, Dai H and Li M 2002 *J. Wuhan Univ. Technol. Mater. Sci.* **17** 39
[36] Zhuang Z and Aizawa M 2013 *J. Mater. Sci.: Mater. Med.* **24** 1211
[37] Hung S C, Mathies R A and Glazer A N 1998 *Anal. Biochem.* **255** 32
[38] Warburg O and Christian W 1942 *Biochem. Z.* **310** 384
[39] LeGeros R Z, Bonel G and Legros R 1978 *Calcif. Tissue Res.* **26** 111
[40] Rey C, Collins B, Goehl T, Dickson I R and Glimcher M J 1989 *Calcif. Tissue Int.* **45** 157
[41] Elliott J C 1994 *Structure and Chemistry of the Apatites and Other Calcium Orthophosphates*

(Amsterdam: Elsevier) p 171
[42] Boulos S P, Davis T A, Yang J A, Lohse S E, Alkilany A M, Holland L A and Murphy C J 2013 *Langmuir* **29** 14984
[43] Cheng S, Chittur K K, Sukenik C N, Culp L A and Lewandwska K 1995 *J. Colloid Interface Sci.* **162** 135
[44] Pauthe E, Pelta J, Patel S, Lairez D, Goubard F, 2002 *Biochim. Biophys. Acta* **1597** 12
[45] Chang I, Lin J, Andrade J D and Herron J N 1995 *J. Colloid Interface Sci.* **174** 10
[46] Pickford A R, Smith S P, Staunton D, Boyd J and Campbell I D 2001 *Embo. J.* **20** 1519
[47] Vakonakis I, Staunton D, Rooney L M and Campbell I D 2007 *Embo. J.* **26** 2575
[48] Bencharit S, Cui C B, Siddiqui A, Howard-Williams E L, Sondek J, Zuobi-Hasona K and Aukhil I 2007 *J. Mol. Biol.* **367** 303
[49] Osterlund E, 1988 *Biochim. Biophys. Acta* **955** 330
[50] Kawasaki T, Nikura M and Kobayashi Y 1990 *J. Chromatogr.* **515** 125
[51] Kawasaki T 1991 *J. Chromatogr.* **544** 147
[52] Kandori K, Fudo A and Ishikawa T 2002 *Colloids Surf. B* **24** 145
[53] Guo X and Xiao P 2006 *J. Eur. Ceram. Soc.* **26** 3383
[54] Kadler K E, Hill A and Canty-Laird E G 2008 *Curr. Opin. Cell. Biol.* **20** 495.